Fast and Accurate Simulation Technique for Large Irregular Arrays

Ha Bui-Van, Jens Abraham, Michel Arts, Quentin Gueuning, Christopher Raucy
David González-Ovejero, *Senior Member, IEEE*, Eloy de Lera Acedo,
and Christophe Craeye, *Senior Member, IEEE*

***Abstract*—A fast full-wave simulation technique is presented for the analysis of large irregular planar arrays of identical 3-D metallic antennas. The solution method relies on the Macro Basis Functions (MBF) approach and an interpolatory technique to compute the interactions between MBFs. The harmonic-polynomial model is established for the near-field interactions in a modified system of coordinates. For extremely large arrays made of complex antennas, two approaches assuming a limited radius of influence for mutual coupling are considered: one is based on a sparse-matrix LU decomposition and the other one on a tessellation of the array in the form of overlapping sub-arrays. The computation of all embedded element patterns is sped up with the help of the non-uniform FFT algorithm. Extensive validations of this new approach, named HARP, are shown for arrays of log-periodic antennas envisaged for the low-frequency SKA (Square Kilometer Array) radio-telescope. The analysis of SKA stations with such a large number of elements has not been treated yet in the literature. Validations include comparison with results obtained with commercial software and with experiments. The proposed method is particularly well suited to array synthesis, in which several orders of magnitude can be saved in terms of computation time.**

***Index Terms*—Irregular antenna arrays, wideband arrays, full-wave simulation, Method of Moments, Macro Basis Functions (MBF), Square Kilometer Array (SKA).**

I. Introduction

MODERN radars [1], massive MIMO [2] and radio astronomy arrays [3], [4] are in need of accurate modeling of their main electromagnetic properties. These are strongly impacted by mutual coupling and include the array impedance matrix and all embedded element patterns (EEP), i.e. the patterns of each individual elements in the presence of all other antennas. This can become a challenging task, knowing that arrays can consist of hundreds or thousands of elements, as considered in the SKA project [5], [6] and in modern radar systems [1].

H. V. Bui, Q. Gueuning, C. Raucy and C. Craeye are with the ICTEAM, Université catholique de Louvain, 1348 Louvain-la-Neuve, Belgium e-mail: (buivanha@uclouvain.be, christophe.craeye@uclouvain.be).

J. Abraham was with Astrophysic Group, Cavendish Laboratory, University of Cambridge. He is now with the Department of Electronic Systems, Norwegian University of Science and Technology, Trondheim, Norway.

E. de Lera Acedo is with Astrophysic Group, Cavendish Laboratory, University of Cambridge.

M. Arts is with ASTRON, the Netherlands.

David González-Ovejero is with Institut d'Électronique et de Télécommunications de Rennes (IETR, UMR CNRS 6164), Université de Rennes 1, 35042 Rennes, France (david.gonzalez-ovejero@univ-rennes1.fr).

Manuscript received Feb. 01, 2017, revised Oct. 16, 2017, accepted Feb. 03, 2018.

The arrays can be regular as well as non-regular. Irregular arrays exhibit a series of advantages over regular arrays, namely the randomization of the side-lobes and of the mutual coupling effects [7]. Both of these factors allow the operation of the arrays over a much larger frequency band compared to traditional regular arrays [8], with a limited number of elements. The accurate knowledge of the antenna and array beams, as well as of the elements' impedance in the presence of mutual coupling [9] is essential for the design of these systems, i.e. for the design of the antenna elements, the array configuration and the electronics connected to the antennas, especially the first stage amplification. The number of elements in the arrays, the geometrical complexity of the elements and the electrical size of these systems represent a challenge regarding their computer modeling. In particular, the irregularity of the elements' positions in the array prevents us from using certain approximations, such as periodic boundary conditions possibly combined with corrections for truncation [10]. The present paper proposes a solution based on two novel contributions: (1) firstly, a fast full-wave technique relied on the harmonic polynomial representation of interactions between antennas with a new change of variables versus radial coordinate to accurately and efficiently simulate large irregular arrays of complex structures; and (2) a tessellation scheme that exploits this fast simulation technique and the partition of the arrays into non-overlapping subarrays for the analysis of extremely large arrays consisting of hundreds or thousands of elements. The exploitation of the Nonuniform-FFT (NFFT) also vastly accelerates the computation of the embedded element patterns.

Integral equation techniques solved with the method of moments (MoM) are very convenient for antenna problems, since they inherently account for radiation. However, when one uses Gaussian elimination, the MoM solution has a complexity of $O((N_a N_e)^3)$, where N_a is the number of antennas in the array, and N_e is the number of elementary basis functions per element. For large arrays of complex antennas, the multilevel fast multipole (MLFMA) technique [11], and its hybridization with other techniques (e.g. HOMoM-MLFMA [12]) are often exploited in an iterative scheme. Unfortunately, the calculation of the array impedance matrix and all EEPs in large finite arrays requires a new series of iterations for excitation at each antenna port. This often leads to an unaffordable computational effort for large arrays, besides the uncertainty related to the number of iterations. A non-iterative technique is then favorable, provided that it can benefit from the proper

compression of unknowns and from further accelerations. That is the case for techniques such as Macro Basis Functions (MBF) [13], Characteristic Basis Functions (CBF) [14], [15], Synthetic Function Expansion (SFX) [16], [17], or entire/sub-entire-domain (SED) basis functions [18], [19].

MBF-type techniques achieve a compression of the MoM impedance matrix by replacing the original set of elementary basis functions by a new set of functions obtained through the solution of smaller problems. Once the MoM matrix size is reduced by means of the MBF technique, the $O((N_a N_e)^3)$ complexity for solving the system of equations is reduced to $O((N_a N_m)^3)$, where N_m is the number of MBFs and $N_m << N_e$. Nevertheless, the impedance matrix filling time remains $O((N_a N_e)^2)$, the same as for the original MoM, which is prohibitive for large arrays. To overcome this obstacle, different techniques have been proposed, such as the multipole expansion algorithm [20], [21], the interpolatory technique [22], the perturbation technique based on the domain Green's function [23] and its enhanced version using the adaptive cross approximation (ACA) [24], or the combination of multipole and Contour-FFT approaches for printed structures [25]. The multipole expansion, however, suffers from the instability of near-field interaction, which appears when antennas are too close to each other, i.e. for distances smaller than about one wavelength. For dense wideband arrays, such as those envisaged for the SKA, antennas are very close to each other at low-frequencies, which requires additional efforts to explicitly calculate the near-field interactions. In this respect, the interpolatory technique presented in [22] is very effective in providing highly accurate solutions even in the near-field [26]. Moreover, MBF interactions are rapidly evaluated from a model, which is built beforehand and is independent of the array configuration. The method, renamed later as HARP [27], has shown great capability and has been extended to the analysis of antennas made of wires, in order to model the SKA1-Low arrays [8], [28].

Preliminary results of HARP on SKA1-Low antennas have been presented in recent conference papers [26], [27], [29]. Nonetheless, limited details were presented about the technique itself and its performance. The present paper further extends this method including a detailed description of the proposed technique, new improvements and extended validation. HARP is now capable of simulating SKA stations over the whole frequency band (50 MHz to 350 MHz) in a matter of minutes for each frequency point. From now on the name HARP refers to the whole method that includes all novel contributions described in this paper.

Additionally, two approaches are presented to exploit the fast simulation method for the analysis of extremely large arrays, namely, the sparse matrix approach and the tessellation approach. These methods make use of the so-called radius of influence (RI) concept, which is often applied to the analysis of large arrays [30]. The first approach calculates only the interaction between antennas whose relative distance is smaller than the RI, which leads to a sparse interaction matrix that can be effectively LU-decomposed and solved exploiting sparse-matrix libraries. In the tessellation approach, the full array is first partitioned into overlapping subarrays. The EEPs are retained only for the internal (or non-overlapping) part of the subarray. The size of the internal part and of the extended surrounding area of the subarray are determined so as to minimize the computational cost. As each subarray can be analyzed independently, this approach enables the simulation of very large arrays of complex elements on a normal desktop computer; it also facilitates parallel implementation. Finally, as explained above, the MBF approach allows the fast calculation of induced currents for excitation at each port. The calculation of corresponding EEPs is then expressed as superposition of pattern multiplication problems, one per MBF [31], and the array factors calculation is accelerated using the non-uniform FFT (NFFT) [31] – [33].

In this paper, the SKA1-Low arrays are taken as a case study to extensively validate the performance of HARP. Upon its completion, the SKA1-Low instrument will consist of 512 stations, each with 256 log-periodic antennas (SKALA) [8], [28], (see Fig. 1), arranged in a pseudo-random configuration, as shown in Fig. 2. With an ultra-wideband characteristic (7:1 fractional bandwidth) and its complex structure, the modeling and simulation of the SKA1-Low frequency array presents a challenge as the array is quite dense at low frequencies, while at high-frequencies, the antenna needs to be meshed precisely. The accurate modeling of the SKALA antenna has a strong impact on the results obtained with a given simulation software. The results obtained using HARP will be validated with those calculated using commercial software on the SKA-station, and with measurements of the isolated elements and a small 3×3 array.

The remainder of the paper is organized as follows. In Section II, the fast full-wave technique and the strategies to analyze extremely large arrays are detailed. In Section III, numerical results for the SKA1-Low case are presented, with data obtained using HARP, CST Studio [34], WIPL-D [35], and measurements for self-impedance and coupling in a small array. In Section IV, the performance of the tessellation scheme on very large arrays is examined and compared with those from the traditional RI approach on different arrays of SKALA antennas. Finally, conclusions are drawn in Section V.

II. Fast Full-wave Technique

In this section, we will explain in detail the HARP method, and present improvements that enable HARP to analyze large random arrays made of complex radiators, such as the SKALA antenna. The tessellation approach, which exploits the fast interaction model, is also introduced; it enables the effective simulation of extremely large arrays. For the sake of clarity, the interpolatory method is first recalled. Interested readers are referred to [22] for detailed explanations regarding the interpolatory technique. In the present work, the MBFs are obtained using the "primary-and-secondaries" approach [14], where the primary MBF corresponds to the current distribution on an isolated element and the secondary MBFs are the currents induced on a set of neighboring antennas by the element that supports the primary MBF.

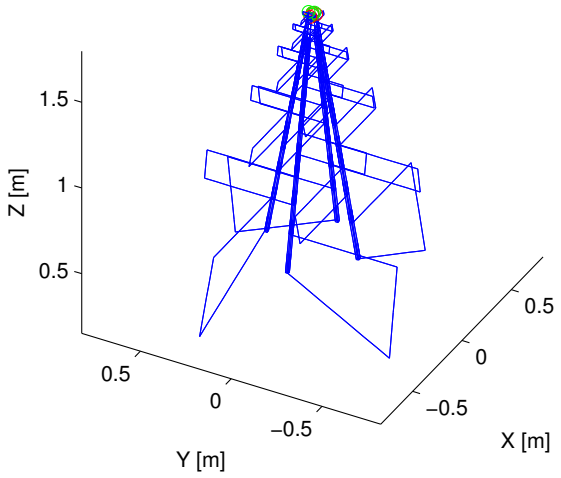

Fig. 1. Wire mesh of the SKA Log-periodic Antenna (SKALA) having a footprint of 1.2×1.2 m^2. The SKALA consists of 4 arms supported by 4 spines, with two orthogonal feeds (on top), providing two polarizations.

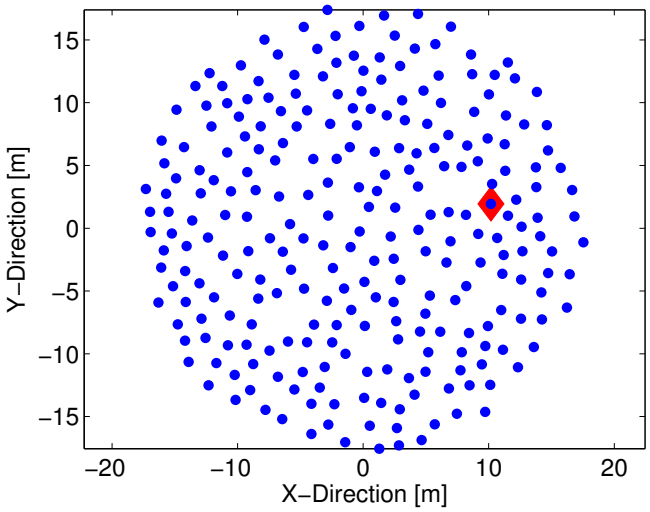

Fig. 2. Layout of a SKA1-low station consisting of 256 SKALA antennas with a minimum distance of 1.35 m.

A. Background of HARP

The interpolatory approach was proposed in [22] to quickly compute the interaction matrix between MBFs, which are the entries of the reduced MoM matrix. The interaction between a source MBF S on antenna n placed at the origin and a testing MBF T on antenna m, positioned at $(r_{mn}, \hat{\alpha})$, was first approximated as

$$Z_{\mathrm{TS}}^{\mathrm{app}}(r_{mn},\hat{\alpha}) \approx -j\omega\mu\ \vec{F}_{T,m}^{\hat{\alpha},*}\ .\ \vec{F}_{S,n}^{\hat{\alpha}}\ \frac{e^{-jkr_{mn}}}{4\pi r_{mn}} \tag{1}$$

where $\hat{\alpha}$ points from the reference point in the source antenna to the reference point in the testing antenna and r_{mn} represents the inter-element distance, ω is the angular frequency, μ is the free-space permeability, $\vec{F}_{T,m}^{\hat{\alpha}}, \vec{F}_{S,n}^{\hat{\alpha}}$ are the radiation patterns of the testing and source MBFs, respectively, and $(*)$ stands for complex conjugate. The actual interaction is then obtained as a sum of the above far-field approximation and a complementary part, which is represented using a harmonic-polynomial model. The model is built by firstly calculating explicitly the exact interaction between MBFs over a grid with a limited number of points. A mathematical representation of the difference between the exact and far-field approximated interaction is then constructed after phase correction and an appropriate change of variables. The first two steps can be expressed in a compact form as

$$B_{\mathrm{TS}}(r_{mn},\hat{\alpha}) = \frac{Z_{\mathrm{TS}}^{\mathrm{exact}}(r_{mn},\hat{\alpha}) - Z_{\mathrm{TS}}^{\mathrm{app}}(r_{mn},\hat{\alpha})}{e^{-jkr_{mn}}} \tag{2}$$

where $Z_{\mathrm{TS}}^{\mathrm{exact}}(r_{mn},\hat{\alpha})$ is the exact interaction explicitly calculated on a pre-defined polar-radial grid. The numerator of Eq. (2) is the far-field subtraction operation, while the denominator stands for the phase correction step. The result of Eq. (2) is then modeled in a harmonic-polynomial form [22] with a proper change of variables, i.e. $d = 1/r^2$:

$$B_{\mathrm{TS}}(d,\hat{\alpha}) = \sum_{p=-P}^{P} e^{jp\alpha} \sum_{q=0}^{Q} c_{pq}\ d^q \tag{3}$$

where P and Q are the orders of Fourier Series and polynomial, respectively, and c_{pq} are coefficients calculated in the least-squares sense. Once the model has been built, the interaction between MBFs is rapidly calculated by adding up the far-field contribution and the complementary part evaluated from the model.

$$Z_{\mathrm{TS}}(r_{mn},\hat{\alpha}) = Z_{\mathrm{TS}}^{\mathrm{app}}(r_{mn},\hat{\alpha}) + B_{\mathrm{TS}}(r_{mn},\hat{\alpha})e^{-jkr_{mn}} \tag{4}$$

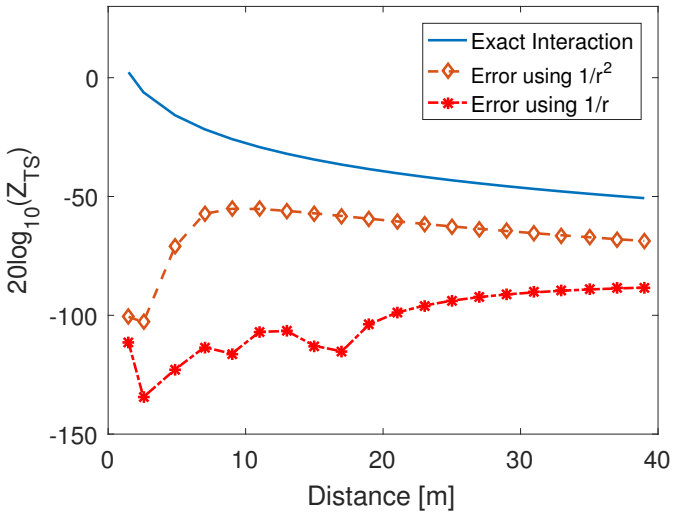

Fig. 3. Interaction between two primary MBFs on two SKALA antennas with a source antenna (S) at the origin and a test one (T) moving along X-axis at 110 MHz. Error is evaluated between the exact interaction and the interaction obtained by HARP with $1/r^2$ and $1/r$ change of variable. Error is calculated as $20\log_{10}|Z_{\mathrm{TS}}^{\mathrm{exact}} - Z_{\mathrm{TS}}^{\mathrm{HARP}}|$.

B. Improved model for MBF interactions

Improvements have been introduced to the original version of HARP to capture the interaction of complex structures such as the SKALA element. The first enhancement appears at the change of variables step, where $d = 1/r$ is now implemented

instead of $d = 1/r^2$ as in Eq. (3). This modification is physically interpreted as taking into account not only the contribution of $1/r^2$, but also of $1/r^3$ field components [36], which are non-negligible in the case of SKALA. Such a change of variables is also consistent with the multipole-based model in [26], where a Laurent series versus the r variable is obtained. The latter work, however, suffers from the stability issues in the very near field. Therefore, in this case, we followed [22] to build the interaction model using the new change of variables.

The improvement in the accuracy of HARP using $1/r$ change of variables is illustrated in Fig. 3, where the interaction between two primary MBFs are calculated for varying distance at 110 MHz. Both versions of HARP can capture the near-distance interaction, while only the $1/r$ change of variables allows the HARP method to model much more accurately the interaction from very small to far distances. The same improvement is observed at other frequencies. This enhancement enables the proposed method to capture precisely mutual coupling in large random arrays. It is noted that the interaction models are constructed using the same number of coefficients for both cases (i.e. $1/r$ and $1/r^2$ change of variables).

Additionally, improvements have been added to the implementation of HARP. The DFT approach has been used instead of a least-squares estimator to obtain the harmonic coefficients (c_{pq}). Also, the sampling points on the grid are determined by an appropriate sampling routine, i.e. a regular grid on angular variable, and inversely regular along the radial distance (regular in $1/r$ scale). Lastly, it is noticed that the interpolation from HARP model via (3) is carried out for every pair of MBFs using two summations. This step is accelerated by writing (3) as a vector-matrix-vector product in MATLAB® [37] implementation (i.e. the left vector is a row-vector of Fourier series, the center matrix is the matrix c_{pq}, and the right vector is a column of polynomials order Q).

Regarding the computational aspect using HARP, the complexities for filling the reduced matrix and solving the system of equations are $O(N_a^2 N_m^2 S)$ and $O((N_a N_m)^3)$, respectively, where S is a small factor related to the calculation of Eq. (4) [22]. The number of MBFs is generally smaller by about two orders of magnitude than the number of basis functions used to describe the current on the antenna (related to meshing); the drastic reduction in the number of unknowns enables the acceleration of the analysis using HARP. In [22], it is shown that interpolatory (or HARP) technique is more efficient than the multipole expansion [20]. Moreover, HARP is able to accurately evaluate the near-field interaction for closely packed arrays.

C. Fast Pattern Calculations: N-FFT

The use of MBFs allows one to write the pattern of each antenna as a sum of MBF patterns multiplied by the corresponding coefficients for the MBF. Hence, the array pattern can be expressed as:

$$\vec{F}_{array}(\theta,\phi) = \sum_{i=1}^{N_a}\sum_{j=1}^{N_m} c_{ij}\,\vec{F}_j(\theta,\phi)\,e^{jk(u_x x_i + u_y y_i)} \quad (5)$$

$$= \sum_{j=1}^{N_m} \vec{F}_j(\theta,\phi)\sum_{i=1}^{N_a} c_{ij}\,e^{jk(u_x x_i + u_y y_i)} \quad (6)$$

where (x_i, y_i) is the position of the i^{th} antenna, $\hat{u} = (u_x, u_y, u_z)$ is a unit vector in the direction (θ,ϕ) of interest, $\vec{F}_j(\theta,\phi)$ is the pattern of MBF j, and c_{ij} is the coefficient for MBF j on antenna i. The swapping of the summations is possible since only one set of MBFs is used for all-identical-antennas of the array. As the MBF patterns in Eq. (6) are factored out, the second summation becomes the array factor, which can be rapidly evaluated using the N-FFT [32], [31], [33] for irregular arrays. It is noted that since the MBF patterns are smooth functions, they are evaluated over a much sparser grid in advance. The higher resolution patterns then can be rapidly obtained using 2-D interpolation on the grid used for the N-FFT. This approach is also applied for the calculation of each EEP of the array, where the induced currents are quickly calculated for excitation at a given antenna port.

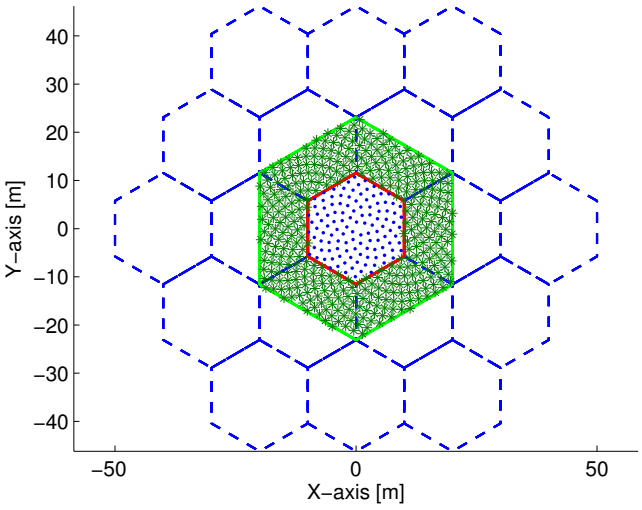

Fig. 4. Tessellation (subarray) approach: inner non-overlapping part (blue dashed hexagonal) and an extended area limited to the green hexagonal.

D. Analysis Schemes for Very Large Arrays

For extremely large arrays, comprising thousands of antennas, the direct implementation of HARP on the whole array would require too much memory and computation time. An effective approach exploiting HARP for such arrays is then needed. Generally, the so-called radius of influence (RI) concept is often applied [30], [23] for the analysis of very large arrays; here the interactions are only considered when the separation between elements is smaller than the RI. This results in a sparse matrix for the reduced MoM system of equations. The filling time of this sparse matrix and the solution time of the system of equations are significantly reduced owing to the use of sparse operations. More precisely,

sparse matrix libraries [38] are applied to obtain a sparse LU-decomposition of the matrix. Fast solutions can then be computed for any excitation law. The approach, however, requires a large RI [30] in order to obtain a highly accurate pattern, which implies an increase of the computational cost.

An alternative technique is proposed below; it relies on the tessellation of the array into subarrays. The RI concept is then applied to each subarray individually. The idea is illustrated in Fig. 4, where the elements in the array are clustered into subarrays, i.e. hexagonal shapes with the inner non-overlapping part of radius $\mathrm{R_{in}}$ (dashed blue line), and an extended area between the inner radius $\mathrm{R_{in}}$ and the outer one $\mathrm{R_{in}} + \mathrm{R_{ext}}$ (green area). To analyze the original array, each subarray is considered separately including the inner and the outer parts. The new interaction model described in Section II-B is then called to rapidly obtain the interaction matrix for a subarray. The MBF-currents and EEPs are calculated by exciting only elements within the inner part while terminating the elements in the outer part. It should be noted that only EEPs of elements within the inner part are retained. The tessellation approach deals with subarrays having much smaller size than the whole array, which will ease the computational effort of solving the MoM system of equations. The use of an outer part with a width of $\mathrm{R_{ext}}$ at least equal to $\mathrm{R_{in}}$ helps to increase the accuracy of the results.

An optimal choice of $\mathrm{R_{ext}}$ can be made by analyzing the computational complexity of the approach. Assuming that a random array has a constant antenna density, the number of antennas on a subarray (inner and outer parts) will be proportional to $(\mathrm{R_{in}} + \mathrm{R_{ext}})^2$. The number of subarrays will be of order of $N_a/\mathrm{R_{in}^2}$. Following the calculation in [22], the computational complexity for filling the matrix can be expressed as a function of $\mathrm{R_{in}}$:

$$C = \alpha \frac{N_a}{\mathrm{R_{in}}^2} (\mathrm{R_{in}} + \mathrm{R_{ext}})^4 \tag{7}$$

where α is a constant taking into account all other constant factors such as the number of MBFs. C presents a minimum when $\mathrm{R_{in}} = \mathrm{R_{ext}}$. The same minimum can be found regarding the complexity of solving the system of equations. This gives a rule of thumb for the choice of $\mathrm{R_{in}}$ and $\mathrm{R_{ext}}$ so as to optimize the quality of the solution while minimizing the computational complexity.

One of the important advantages of HARP is the re-usability of the interaction model, which is established only once and can be exploited to analyze any array made of the same element. This feature is very helpful for the tessellation approach, as in this scenario, several subarrays can be simulated separately, which straightforwardly allows parallelization. The implementation and evaluation of HARP using the sparse matrix and tessellation approaches will be studied in Section IV.

III. Numerical and Experimental Validation

Preliminary data at a single frequency has been presented in recent conference papers [27], [29] with limited results on relatively small arrays and on a SKA1-Low station. In the present paper, the performance of HARP is studied in depth on several examples, which include an isolated antenna, a small compact array, and the SKA station, shown in Fig. 2, at 50 MHz, 110 MHz, 200 MHz and 350 MHz, covering the whole SKA1-Low band. Simulated results from two com-

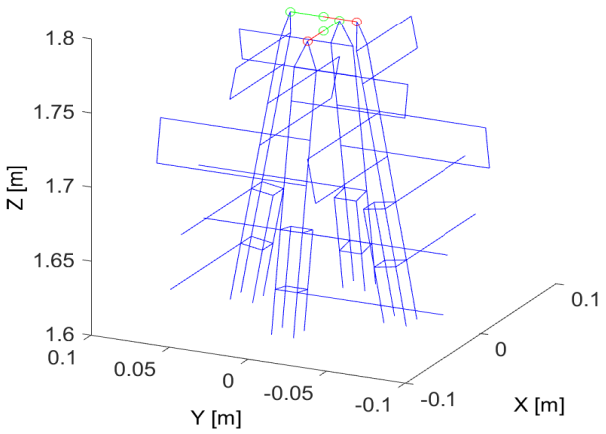

Fig. 5. Zoom in of the upper part of the SKALA mesh implemented in this work: 2 feed points on top and 4 cages at the bottom.

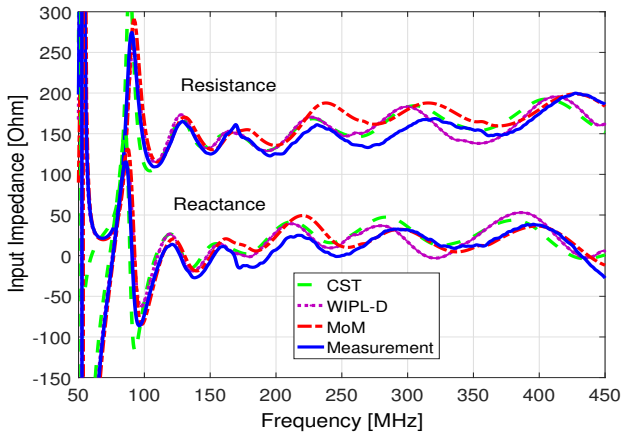

Fig. 6. Real and imaginary parts of the self-impedance of SKALA. Measurement with antenna standing on a 2 m square metallic ground.

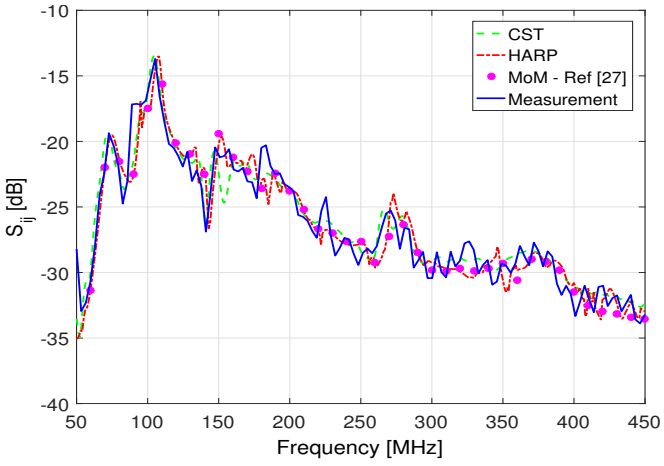

Fig. 7. Coupling coefficient in a 3×3 array, between center element and middle of edge.

mercial software, CST Microwave Studio [34] and WIPL-D [35], are taken as a reference to examine the performance of HARP, while measured data is presented whenever they are available. Different parameters are analyzed, including input impedance, coupling coefficients, EEPs and array patterns. In all cases, the data for one polarization is shown, while the results for the other polarization have the same quality and are not shown. The SKALA model used in HARP consists in a wire mesh comprising 1218 basis functions. This HARP implementation is based on a MoM code that considers wires, with the Poklington approximation [39]. The 4 cm diameter tube that supports each arm does not satisfy that approximation in the upper part of the frequency range. Therefore, those tubes have been replaced by wire cages with a square cross-section and a perimeter equal to that of the tube. Fig. 1 shows a global view of the structure, while Fig. 5 shows a zoom near the feed points and near the cage. The numbers of MBFs are 15, 20, 45, 70 at 50 MHz, 110 MHz, 200 MHz and 350 MHz, respectively (linearly scaled versus frequency).

A. Self and Mutual Impedance

Due to the complexity of the design, an accurate model of the SKALA in Fig. 1 is critical for analyzing the performance of the array, e.g. self and mutual impedance are required to study parameters such as noise coupling [40], [41]. The input impedance is then the first parameter to study. Fig. 6 shows the self-impedance simulated using different software, along with the measured data over the low-frequency band. A small deviation of the order of 20 Ω is seen around 200–300 MHz between the simulations and the measurements. This can be attributed to the fact that different software packages model and mesh the SKALA differently, and that the SKALA in the measurement had a metallic ground limited to 2 m, whereas the simulations assume an infinite ground plane. These variations may also explain some of the differences among patterns in the following sections.

Another validation example carries on a 3×3 regular array of SKALAs with element spacing of 1.5 m. The coupling coefficient is calculated between the center antenna and another element at the middle of the edge, as shown in Fig. 7. This example is a repetition of an example in [27], where the solution of the traditional wire-MoM, without acceleration, is reported. Fig. 7 shows that results obtained using HARP and MoM are extremely close, which confirms the accuracy of the HARP method w.r.t. the traditional wire MoM method. Moreover, the HARP and CST simulations follow well the measurement across the whole frequency band.

The mutual impedance is studied for the SKA station as well. Fig. 8 plots the real and imaginary parts of the mutual impedance Z_{ij} for different frequencies in a SKA station between an arbitrary antenna i (a red dot in Fig. 2) and another antenna j running from 1 to 256; the obtained values are sorted versus distance to antenna i. A good agreement is found between HARP and WIPL-D for coupling between antennas. The main difference regards the self-impedance, i.e. zero distance, which is also illustrated in Fig. 6. The results confirm the capability of the current version of HARP to capture the interaction between SKALA antennas in their array environment.

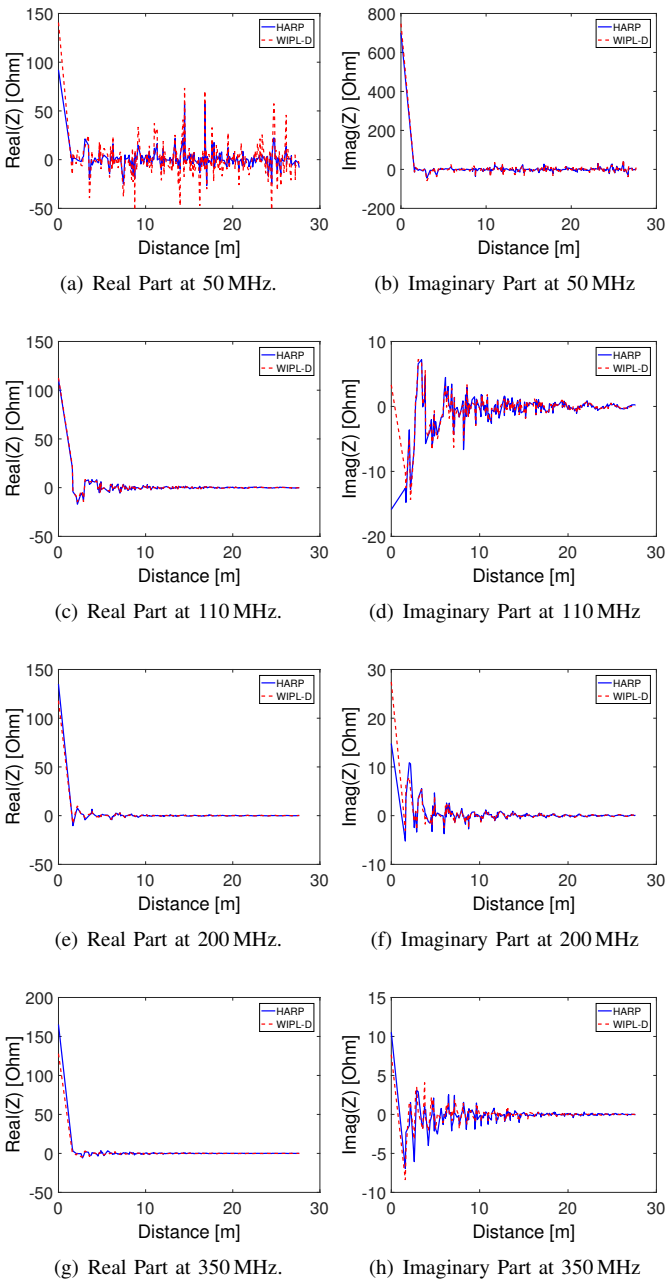

(a) Real Part at 50 MHz. (b) Imaginary Part at 50 MHz

(c) Real Part at 110 MHz. (d) Imaginary Part at 110 MHz

(e) Real Part at 200 MHz. (f) Imaginary Part at 200 MHz

(g) Real Part at 350 MHz. (h) Imaginary Part at 350 MHz

Fig. 8. Mutual impedance of a random antenna i in the SKA station (a red dot in Fig. 2) and other antennas j sorted by the distance to antenna i.

B. Embedded Element Patterns

In applications such as the SKA telescope, the EEPs are of primary interest as they allow one to form different beams collecting signal from sky. An accurate and effective calculation of all EEPs is then required, while taking into account the mutual coupling. In this section, the quality of EEPs obtained using HARP is evaluated. A small testbed of 16 SKALA elements is first analyzed, where the EEPs of all elements are calculated at all frequencies with 1 MHz frequency steps. Then, the SKA station in Fig. 2 is simulated

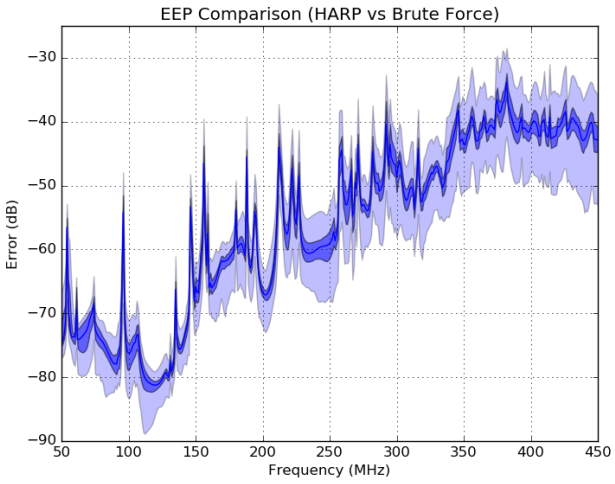

Fig. 9. Error of the EEPs between the HARP and the brute force solution over all 16 antennas in all directions against frequency. The median, 25 % and 75 % percentiles as well as the minimum and maximum error are shown by the blue line, the dark blue shaded and the light blue shaded areas, respectively.

at four different frequencies, i.e. 50 MHz, 110 MHz, 200 MHz and 350 MHz, using HARP and WIPL-D, and the calculated EEPs are compared.

1) EEPs of A Small Array: The performance of HARP has been tested against the brute force MoM solution of a small array of 16 SKALA elements for the frequency band (50 – 450 MHz). The array corresponds to a testbed for SKA1-Low technology and is situated at the Mullard Radio Astronomy Observatory (MRAO) near Cambridge, UK [8]. This array with only 16 elements is in a pseudo-random configuration, such as that of SKA stations, and has the same expected element density, with an average inter-element spacing of half wavelength at 77 MHz. The error between the patterns is calculated as:

$$\epsilon = \sqrt{\left|E_\theta - E_\theta^{ref}\right|^2 + \left|E_\phi - E_\phi^{ref}\right|^2} \tag{8}$$

where E and E^{ref} being the EEP calculated by HARP and brute-force MoM with the electric fields being normalized by the maximum of the isolated antenna pattern. This error is calculated in all directions for all involved antennas. The condensed result is shown in Fig. 9 by calculating the percentiles of the error and plotting them over frequency. The HARP method shows very good accordance to the brute-force MoM results over the whole frequency range. The error increases at the highest end of the band, but it is still below -30 dB.

2) EEPs of SKA station: The performance of HARP on the SKA station is now validated with patterns simulated using the WIPL-D software [35]. The EEP of an arbitrary element (red dot in Fig. 2) obtained using HARP is taken as an example. Fig. 10 shows the EEPs at four different frequencies and their differences w.r.t. WIPL-D, where the error patterns are computed using (8) with E and E^{ref} being patterns obtained using HARP and WIPL-D, respectively. An excellent agreement is shown at low-frequencies, where the difference level is found below -30 dB at 50 MHz. The variation becomes

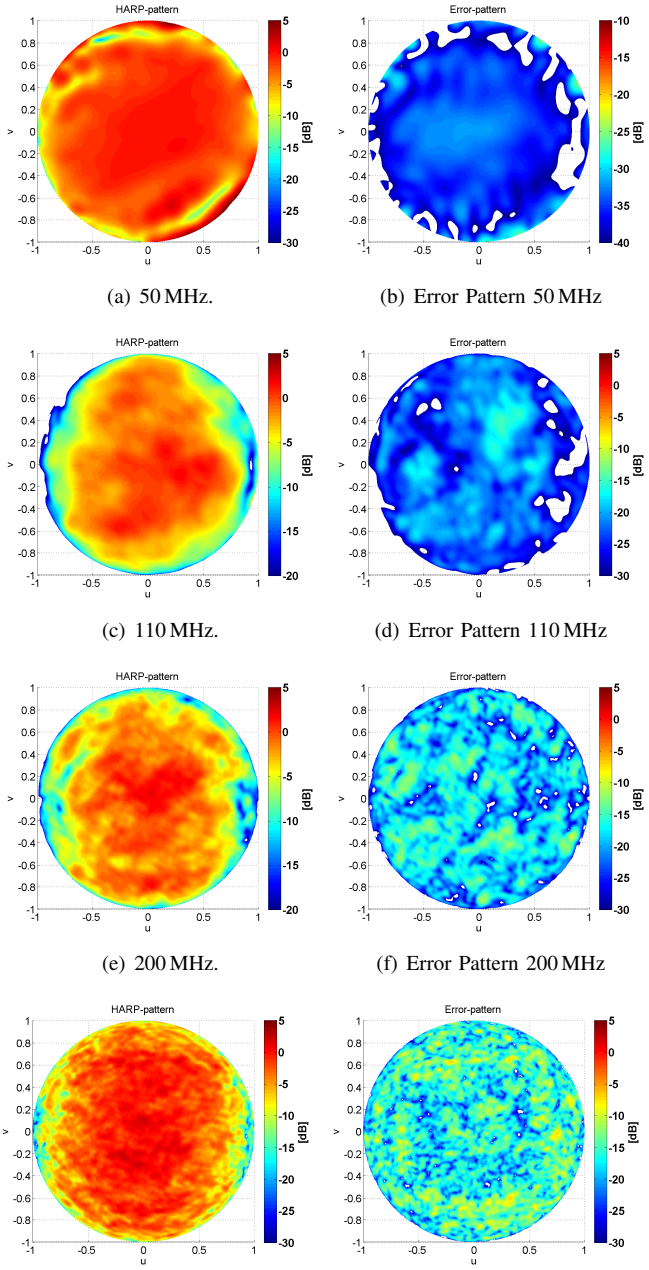

(a) 50 MHz. (b) Error Pattern 50 MHz

(c) 110 MHz. (d) Error Pattern 110 MHz

(e) 200 MHz. (f) Error Pattern 200 MHz

(g) 350 MHz. (h) Error Pattern 350 MHz

Fig. 10. EEP obtained by HARP and the difference w.r.t. WIPL-D of a random element in the SKA station (red dot in Fig. 2).

more visible as the frequency increases. A detailed study of the performance of different software at 350 MHz is carried out on an array of 2 antennas positioned along the $x-$axis with varying distance. The EEPs obtained using CST, WIPL-D, brute-force MoM and HARP are plotted together in Fig. 11 for a separation equal to 8 m. For this 2 element array, the EEPs are similar to the isolated pattern, and mutual coupling clearly appears as ripples in the main beam. The results show that while the mutual coupling is accounted for in all software packages, a small difference is observed in the EEPs. The reason is attributed to the difference in the geometrical modeling of the SKALA, i.e. the use of different meshes

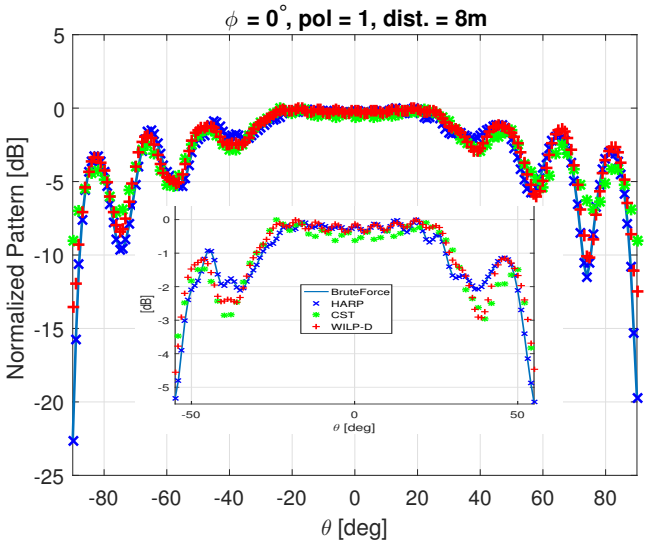

Fig. 11. $\phi = 0°$ cut of one EEP in an array of 2 SKALA at a distance of 8m for the first polarization at 350 MHz. (Inset: zoom in of the main beam)

in each software, which leads to differences in the isolated pattern. At the highest frequency, a small difference in antenna modeling will result in a significant variation in the radiation patterns. This explains the discrepancies in the EEPs visible in Fig. 10(h), as well as the self-impedance behavior in Fig. 6. A stronger indicator that the discrepancies mainly come from the mesh is that the errors in the isolated pattern are almost as large as in the EEPs. Moreover, it is important to note that, in Fig. 11, patterns calculated using brute-force MoM and HARP overlap very well, which confirms the accuracy of the HARP method.

C. Array Patterns

In this section, the EEPs calculated using HARP and WIPL-D software are exploited to form the array pattern. A simple beamforming method is implemented with uniform excitation and scanning at broadside. Fig. 12 shows the radiation pattern of the SKA station at different frequencies in two principal planes calculated using HARP and WIPL-D. The two methods show a great agreement across the frequency band, as the difference in patterns, evaluated by (8), is only shown at a -30 dB level, except for the highest frequency, i.e. 350 MHz, where the error in the main beam is near -24 dB. As explained above, the visible difference in the patterns at higher frequency is due to the difference in modeling of the SKALA in the two software. To demonstrate the impact of the isolated element modeling, we show that it can be partially undone by properly adding the difference of isolated patterns between HARP and WIPL-D into the EEPs, as shown in Fig. 13. A better agreement is clearly seen w.r.t. Fig. 12(d), especially near the main beam. This exercise illustrates that the difference between WIPL-D and HARP at highest frequency is mainly due to the modeling of the SKA antennas in these two software packages. Expectedly, this fine modeling difference becomes more visible at high-frequency.

TABLE I
COMPUTATIONAL TIME OBTAINING EMBEDDED ELEMENT PATTERNS OF A SKA1-LOW STATION AT 110 MHZ

	CST	WIPL-D	HARP
Simulation Time	96 hours	97 hours	0.5 min.

TABLE II
ANALYSIS TIME FOR A SKA STATION USING HARP AT 110 MHZ. (IN SECOND)

Operations	This paper	Ref. [27]
Matrix Filling	10	350
Solving MoM equations	12.6	12.6
Calculation EEPs	6	1234
Total	**28.6**	**1596.6**

Finally, the performance of WIPL-D, CST and HARP for the analysis of a SKA station at 110 MHz is detailed in Table I. A great time saving factor is achieved using the enhanced HARP, while providing highly accurate results, as demonstrated in Fig. 12. The CST simulations were carried out on a server with two processors and two cores each with 384 GB of RAM at the University of Cambridge, UK, whereas the WIPL-D ones were performed on a Windows Server 2008 R2 Enterprise with an Intel Xeon X7550 processor and 125 GB RAM at ASTRON, The Netherlands. All the simulations for HARP were carried out on a desktop computer with 16 GB RAM and Processor Intel Core $i7-3770$ CPU 3.4 GHz at UCL. For HARP, the accounted time stands for matrix filling, solving the system of equations and calculation of all EEPs once the HARP model is built, as reported in Table II. The establishment of the HARP model takes about 3 hours per frequency. It is important to recall that this preparation phase takes place only once and for all, regardless of the array configuration, and can be re-used to analyze any array made of the same element. This feature is very beneficial for simulating SKA arrays, where hundreds of stations are planned, as well as to analyze extremely large arrays, as will be discussed in the next section. It is worth noting that the previous version of HARP [27] took nearly half an hour for the same simulation. The reduction comes from the new implementation of the matrix filling as well as the use of N-FFT pattern calculation as presented in Section II-C. The enhanced HARP also offered more accurate results as shown in Fig. 3 as well as in Fig. 14, where the errors in SKA station pattern using two versions of HARP are plotted. An improvement of 3 dB in the main beam and first sidelobes is observed using $1/r$ change of variables. This enhancement is crucial to accurately analyze the array, especially in the upper frequency band.

IV. SIMULATION OF EXTREMELY LARGE ARRAYS

This section shows the performance of the sparse matrix and tessellation techniques on the analysis of very large arrays. The impact of the Radius of Influence (RI) on the array patterns is studied on arrays of different sizes containing 256, 500, 800, 1000 and 1500 elements. The latter has a diameter of 85 meters, as shown in Fig. 15, and the same

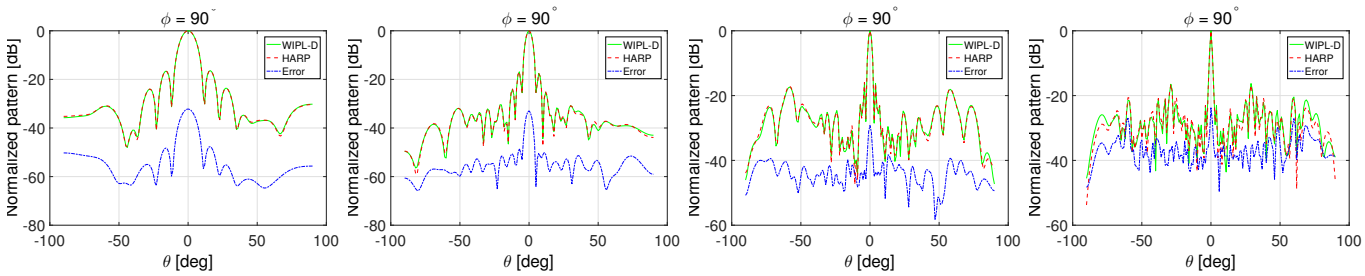

(a) H-plane: $\phi = 90°$, 50 MHz (b) H-plane: $\phi = 90°$, 110 MHz (c) H-plane: $\phi = 90°$, 200 MHz (d) H-plane: $\phi = 90°$, 350 MHz

Fig. 12. Normalized radiation pattern of a SKA station in H-plane ($\phi = 90°$) at different frequencies.

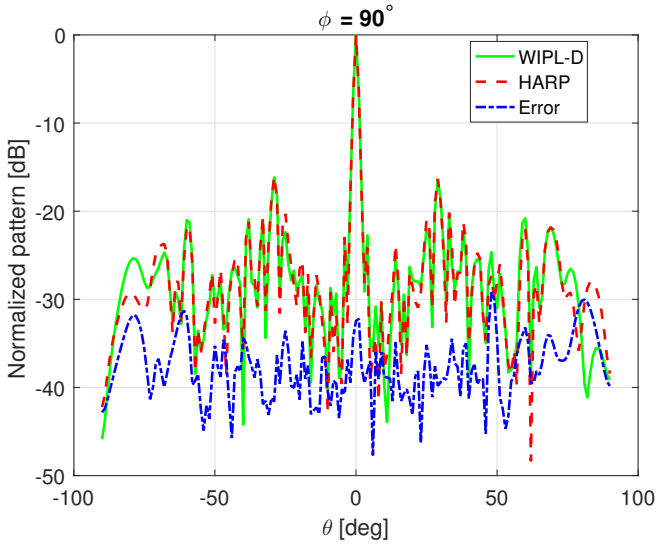

Fig. 13. Normalized radiation pattern of a SKA station at 350 MHz after the difference between isolated pattern is added to all EEPs; in H-plane ($\phi = 90°$) cut.

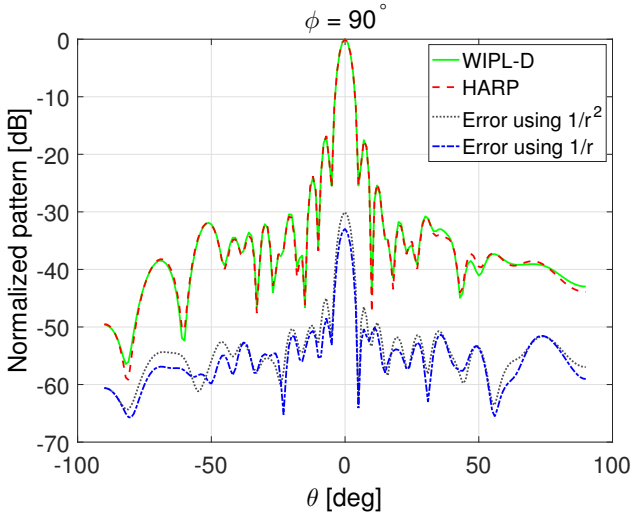

Fig. 14. Array pattern of the SKA station in $\phi = 90°$ plane at 110 MHz and the errors of HARP (w.r.t. WIPL-D) using $1/r^2$ and $1/r$ change of variables.

array density has been considered for all the other arrays. The arrays are simulated at 110 MHz using HARP; EEPs and the array pattern are calculated. It is noted that the array of

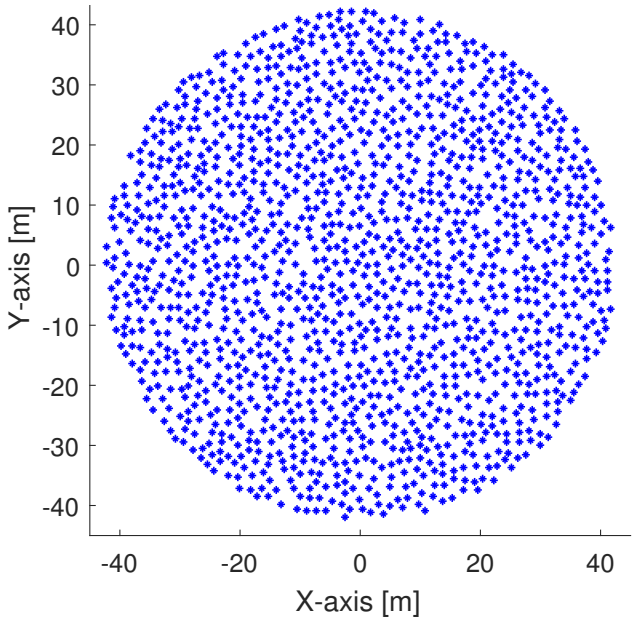

Fig. 15. Layout of 1500 SKALA element array with minimum distance of 1.35 m.

TABLE III
COMPUTATIONAL COMPLEXITY BY SPARSE MATRIX AND TESSELLATION APPROACHES.

	Sparse Matrix	**Tessellation**
Filling Matrix	$\mathcal{O}\left(N_a N_I N_m^2\right)$	$\mathcal{O}\left(N_a N_s N_m^2\right)$
Solving	$\mathcal{O}\left(N_a N_I^2 N_m^3\right)$	$\mathcal{O}\left(N_a N_s^2 N_m^3\right)$

where N_I and N_s are average number of elements within the RI and the subarray, respectively.

1500 elements cannot be handled using CST nor WIPL-D with our current hardware, and the "exact solutions" considered in this section are obtained by simulating the full array without any tesselation (i.e. using only the methods described in Sections II-B to II-C).

A. Sparse Matrix Approach

Fig. 16 shows the exact patterns and the error for different RIs in E-plane ($\phi = 0°$) for the 1500 elements array. The errors are evaluated using (8), where $\overrightarrow{E}(\theta, \phi)$ and $\overrightarrow{E}^{\text{ref}}(\theta, \phi)$ stand for the exact pattern and those obtained using the sparse array approach, respectively. It is clear that for larger values of

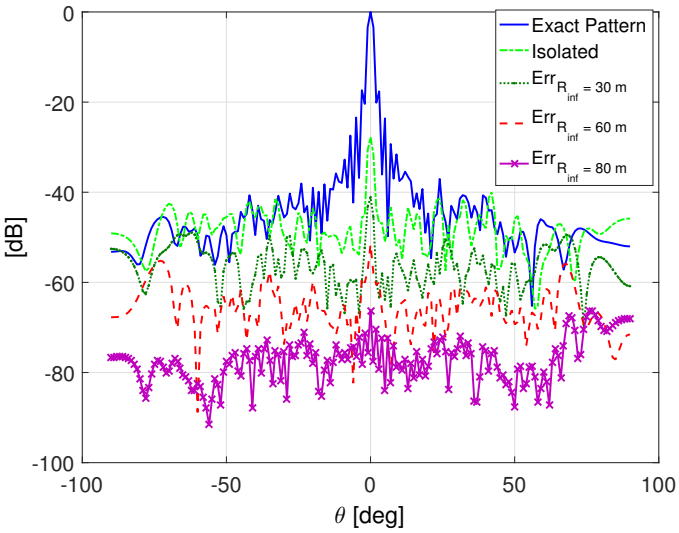

Fig. 16. Normalized radiation pattern of the array in Fig. 15 at 110 MHz in E-plane ($\phi = 0°$) and errors for different RIs in two principal planes using the sparse matrix approach.

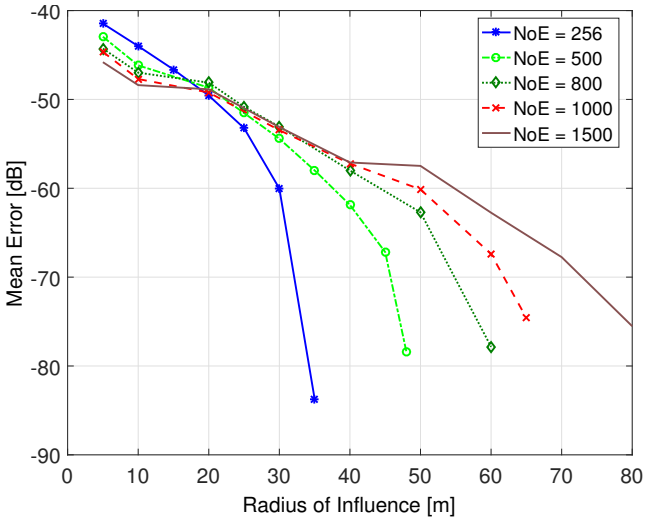

Fig. 17. Mean errors vs. RI for different array sizes using the sparse matrix approach at 110 MHz.

the RI, the errors are smaller, since more elements are included in the RI region. It is also seen that, using only the isolated pattern, the error level is higher than the sidelobe level at far-out angles. Even for RI = 30 m, the error is close to some sidelobes. The results again show the strong effect of mutual coupling in a random array made of SKALA elements. Fig. 17 displays the convergence of error curves versus the RI for different array sizes (i.e. number of elements (NoE) in the arrays are indicated in the legends) at 110 MHz. It shows the trend of reducing errors for larger RI and one can observe that to achieve a given error level, larger arrays require a smaller RI (normalized to array size). This is probably due to the slow averaging effect of randomization of the array on mutual coupling. As the RI is smaller (w.r.t. array size) for large arrays, the interaction matrix will be sparser, which implies the capability to analyze large arrays using the RI concept. The computational complexity of the approach is detailed in Table III, where N_I is the average number of elements within the RI, which is proportional to RI^2.

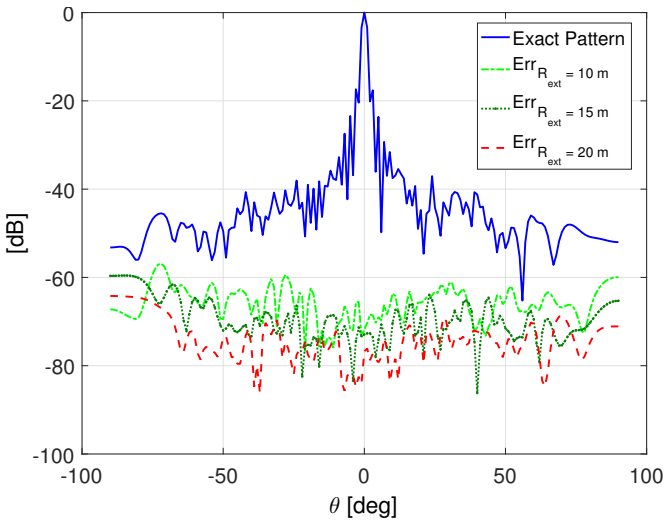

Fig. 18. Normalized radiation pattern of the array in Fig. 15 at 110 MHz in E-plane ($\phi = 0°$) and errors using the tessellation approach in two principal planes.

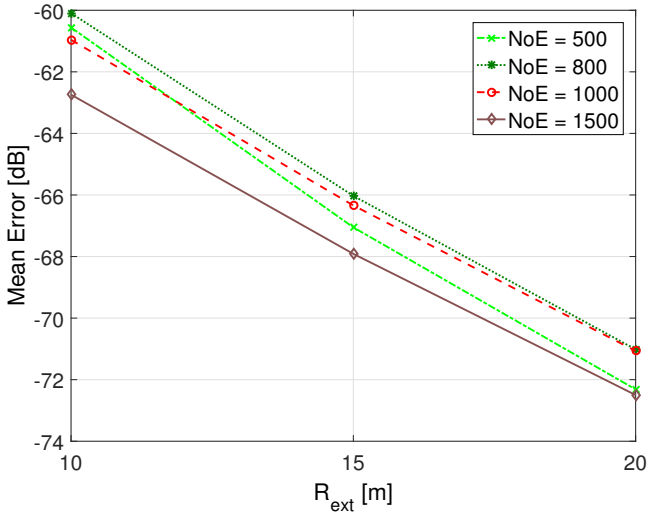

Fig. 19. Mean errors vs. $\mathrm{R_{ext}}$ for different array sizes using the tessellation approach at 110 MHz.

B. Tessellation Approach

Fig. 18 shows the radiation patterns and errors using the tessellation approach on the array of 1500 SKALA elements shown in Fig. 15 for $\mathrm{R_{in}} = 10\,\mathrm{m}$ and different $\mathrm{R_{ext}}$ values. It is interesting to see that tessellation is able to provide high-quality solutions w.r.t. the exact ones as the error levels are quite low even for small $\mathrm{R_{ext}}$. Despite sharing the same RI idea as the sparse array approach, the tessellation seems to perform better. The reason lies in the fact that even if the sparse array approach only accounts for the interaction between elements inside the RI, the solution of the resulting system of equations still provides non-zero currents for elements outside of the RI region, while the excited elements

remain within the RI. This "artificial" current contributes to the radiation patterns, while probably not being highly relevant nor accurate. Conversely, the tessellation approach only solves for the subarray and calculates the contribution of those elements inside the subarray.

Fig. 19 shows the convergence of the tessellation approach for different array sizes. As $\mathrm{R_{ext}}$ increases, the error decreases almost linearly in logarithmic scale. This allows one to obtain a given accuracy by finding a proper $\mathrm{R_{ext}}$. Increasing $\mathrm{R_{ext}}$, however, results in increasing the computational complexity, both for matrix filling and for solving the system of equations. An optimum choice of $\mathrm{R_{ext}}$ can be found following Eq. (7), as discussed in Section II-D; it favors an extended region comprising half of all neighboring inner-hexagons. A detailed complexity of the tessellation approach is listed in Table III, where N_s is the average number of elements in a subarray, which is proportional to $(\mathrm{R_{in}} + \mathrm{R_{ext}})^2$ with $\mathrm{R_{in}} = \mathrm{R_{ext}}$. By selecting N_I and N_s, i.e. choosing RI and $\mathrm{R_{in}}$, respectively, one can obtain a same complexity for both methods. For extremely large arrays, N_I and N_s are at least one order of magnitude smaller than N_a, which results in a big saving factor compared to the direct solution over the whole array.

It is also interesting to see that the convergence curve in Fig. 19 is quite independent from the array size, which assures the performance of the tessellation approach for other (larger) arrays, and allows one to select $\mathrm{R_{in}}$ and $\mathrm{R_{ext}}$ in advance. Regarding the analysis, the tessellation approach offers the possibility of parallelizing the computation as the analysis of each subarray is totally independent. Moreover, the tessellation is not limited by the array size as each subarray can be solved effectively with a present-day desktop computer, providing enough temporary memory RAM to store the reduced MoM matrix and solutions, for example 16 GB has been proven sufficient in all tested cases. For the largest array, i.e. consisting of 1500 SKALA antennas, the analysis took about 15 minutes using the tessellation approach to simulate the array and calculate all the EEPs.

V. Conclusion

A fast full-wave technique for the analysis of large arrays made of complex 3-D metallic antennas has been presented. The calculation of interactions between antennas has been accelerated using the HARP technique, where a non-expensive model is built for MBF interactions. The reduced matrix is then rapidly filled using such model. Several improvements have been added to HARP to cope with the complexity of solving very large arrays. An experimental example of compact array and simulations of SKALA arrays have demonstrated the performance of HARP. Furthermore, the sparse matrix and the tessellation approached have been proposed for analyzing very large arrays of SKALA elements, offering a solution to the analysis of extremely large arrays, such as the SKA telescope, for which hundreds of stations are foreseen. The sparse matrix converged relatively slowly, and required large RIs to achieve accurate result. However, the proposed tessellation approach showed excellent performance for all tested arrays. The approach enables the analysis of very large arrays on present-day desktop computers, while providing highly accurate results.

The simulation technique opens the possibility to integrate the full-wave simulation in an optimization procedure [42], which is capable of taking into account mutual coupling to optimize the performance of the arrays (e.g. in terms of sensitivity, including noise coupling). Moreover, the accurate EEPs obtained using HARP can be incorporated in the calibration stage for modern radars and astronomical instruments such as the SKA. The use of the PMCHWT (Poggio-Miller-Chang-Harrington-Wu-Tsai) approach [43], combined with the surface equivalence principle [44], allows the extension of HARP to antennas comprising dielectric material.

Acknowledgment

The authors would like to thank the UK's STFC funding that has supported this work. They are also grateful to their SKA colleagues for numerous discussions about SKA station modeling.

References

[1] D. Vollbracht, "System specification for dual polarized low power X-Band weather radars using phased array technology," *Int. Radar Conf.,* pp. 1-6, Lille, Oct. 2014.

[2] E. G. Larsson, O. Edfors, F. Tufvesson and T. L. Marzetta, "Massive MIMO for next generation wireless systems," *IEEE Commun. Mag.,* vol. 52, no. 2, pp. 186–195, Feb. 2014.

[3] S. W. Ellingson, "Sensitivity of antenna arrays for long-wavelength radio astronomy," *IEEE Trans. Antennas Propag.,* vol. 59, no. 6, pp. 1855–1863, June 2011.

[4] E. de Lera Acedo, N. Razavi-Ghods, L. E. Garcia, P. Duffett-Smith and P. Alexander, "Ultra-wideband aperture array element design for low frequency radio astronomy," *IEEE Trans. Antennas Propag.,* vol. 59, no. 6, pp. 1808-1816, June 2011.

[5] P. E. Dewdney, P. J. Hall, R. T. Schilizzi and T. J. L. W. Lazio, "The Square Kilometre Array," *Proc. of the IEEE,* vol. 97, no. 8, pp. 1482-1496, Aug. 2009.

[6] The Square Kilometer Array. [Online]. Available: https://www.skatelescope.org/

[7] N. Razavi-Ghods, E. de Lera, A. Makadema, P. Alexander, and A. Brown, "Analysis of sky contributions to system temperature for low frequency SKA aperture array geometries," *Exp. Astron.,* vol. 33, pp. 141 – 155, 2012.

[8] E. de Lera Acedo et al., "SKALA, a log-periodic array antenna for the SKA-low instrument: design, simulations, tests and system considerations," *Exp. Astron.,* vol. 39, no. 3, pp. 567–594, Jul. 2015.

[9] C. Craeye and D. González-Ovejero, "A review on array mutual coupling analysis," *Radio Sci.,* vol. 46, no. RS2012, 2011.

[10] A. Neto, S. Maci, G. Vecchi and M. Sabbadini, "A truncated Floquet wave diffraction method for the full wave analysis of large phased arrays. I. Basic principles and 2-D cases," *IEEE Trans. Antennas Propag.,* vol. 48, no. 4, pp. 594-600, Apr. 2000.

[11] J.-M. Song, W. C. Chew, "Multilevel fast multipole algorithm for solving combined field integral equations of electromagnetic scattering", *Microw. Opt. Technol. Lett.,* vol. 10, no. 1, pp. 14-19, Sep. 1995.

[12] X. Zhao, Z. Lin, Y. Zhang, S. W. Ting and T. K. Sarkar, "Parallel hybrid method of HOMoM – MLFMA for analysis of large antenna arrays on an electrically large platform," *IEEE Trans. Antennas Propag.,* vol. 64, no. 12, pp. 5501-5506, Dec. 2016.

[13] E. Suter and J.R. Mosig, "A subdomain multilevel approach for the efficient MoM analysis of large planar antennas," *Microw. Opt. Technol. Lett.,* pp. 270–277, vol. 26, no. 4, 2000.

[14] S. J. Kwon, K. Du, and R. Mittra, "Characteristic basis function method: a numerically efficient technique for analyzing microwave and RF circuits," *Microw. Opt. Technol. Lett.,* vol. 38, pp. 444–448, Sep. 2003.

[15] R. Maaskant, R. Mittra and A. Tijhuis, "Fast analysis of large antenna arrays using the characteristic basis function method and the adaptive Cross approximation algorithm," *IEEE Trans. Antennas Propag.,* vol. 56, no. 11, pp. 3440–3451, Nov. 2008.

[16] L. Matekovits, V. A. Laza and G. Vecchi, "Analysis of large complex structures with the synthetic-functions approach," *IEEE Trans. Antennas Propag.,* vol. 55, no. 9, pp. 2509–2521, Sept. 2007.

[17] L. Matekovits, G. Vecchi, M. Bercigli and M. Bandinelli, "Synthetic-functions analysis of large aperture-coupled antennas," *IEEE Trans. Antennas Propag.,* vol. 57, no. 7, pp. 1936–1943, July 2009.
[18] W. B. Lu, T. J. Cui, Zhi Guo Qian, Xiao Xing Yin and Wei Hong, "Accurate analysis of large-scale periodic structures using an efficient sub-entire-domain basis function method," *IEEE Trans. Antennas Propag.,* vol. 52, no. 11, pp. 3078–3085, Nov. 2004.
[19] X. Wang, D. H. Werner and J. P. Turpin, "A fast analysis of scattering from large-scale finite periodic microstrip patch arrays arranged on a non-orthogonal lattice using sub-entire domain basis functions," *IEEE Trans. Antennas Propag.,* vol. 62, no. 5, pp. 2543–2552, May 2014.
[20] C. Craeye, "A fast impedance and pattern computation scheme for finite antenna arrays," *IEEE Trans. Antennas Propag.,* vol. 54, no. 10, pp. 3030–3034, Oct. 2006.
[21] D. González-Ovejero, F. Mesa and C. Craeye, "Accelerated macro basis functions analysis of finite printed antenna arrays through 2D and 3D fast multipoles," *IEEE Trans. Antennas Propag.,* vol. 61, no. 2, pp. 707-717, Feb. 2013.
[22] D. Gonzalez-Ovejero and C. Craeye, "Interpolatory macro basis functions analysis of non-periodic arrays," *IEEE Trans. Antenna Propag.,* vol. 59, no. 8, pp. 3117 – 3122, Aug. 2011.
[23] D. J. Ludick, R. Maaskant, D. B. Davidson, U. Jakobus, R. Mittra and D. de Villiers, "Efficient analysis of large aperiodic antenna arrays using the domain green's function method," *IEEE Trans. Antennas Propag.,* vol. 62, no. 4, pp. 1579 – 1588, Apr. 2014.
[24] D. J. Ludick, R. Maaskant, D. B. Davidson and U. Jakobus, "Accelerating the Domain Green's Function Method through adaptive cross approximation," *Proc. Inter. Conf. Electromag. Adv. App. (ICEAA)*, pp. 636-639, Palm Beach, 2014.
[25] S. N. Jha and C. Craeye, "Contour-FFT based spectral domain MBF analysis of large printed antenna arrays," *IEEE Trans. Antennas Propag.,* vol. 62, no. 11, pp. 5752–5764, Nov. 2014.
[26] Q. Gueuning, E. de Lera Acedo, E. Colin-Beltran and C. Craeye, "Mutual coupling analysis of large irregular arrays: from multipole to interpolatory methods," *Proc. 9th Eur. Conf. Antennas Propag.,* Lisbon, 2015.
[27] Q. Queuning, C.Raucy, C. Craeye, E. Colin-Beltran, E. de Lera Acedo, "Mutual coupling analysis in non-regular arrays of SKALA antennas with the HARP approach," *AP-S*, 2015.
[28] E. de Lera Acedo, "SKALA: A log-periodic antenna for the SKA," *Proc. Inter. Conf. Electromag. Adv. App. (ICEAA),* 2012.
[29] H. V. Bui, J. Abraham, Q. Gueuning, E. de Lera Acedo and C. Craeye, "Further validation of fast simulation method at the element and array pattern levels for SKA," *Proc. 10th Eur. Conf. Antennas Propag.,* Davos, Apr. 2016.
[30] E. de Lera Acedo, N. Razavi-Ghods, D. G. Ovejéro, R. Sarkis and C. Craeye, "Compact representation of the effects of mutual coupling in non-regular arrays devoted to the SKA telescope," *Proc. Inter. Conf. Electromag. Adv. App. (ICEAA),* pp. 390-393, Torino, 2011.
[31] C. Craeye, D. Gonzalez-Ovejero, and X. Dardenne, "Efficient numerical analysis of arrays of identical elements with complex shapes," *Jour. Appl. Comput. Electromagn. Soc. (ACES),* vol. 24, no. 2, Apr. 2009.
[32] A. Dutt and V. Rokhlin, "Fast Fourier Transforms for nonequispaced data," *SIAM Journal on Scientific Computing,* vol. 14, no. 6, pp. 1368 – 1393, 1993.
[33] A. Capozzoli, C. Curcio, G. D'Elia, A. Liseno, P. Vinetti, "Fast CPU/GPU pattern evaluation of irregular arrays", *Jour. Appl. Comput. Electromagn. Soc. (ACES),* vol. 25, n. 4, pp. 355–372, Apr. 2010.
[34] CST Microwave Studio, 2015. [Online] Available: https://www.cst.com/
[35] WIPL-D – Electromagnetic Simulation Software [Online] Available: http://www.wipl-d.com/
[36] A. Boag, E. Michielssen and A. Brandt, "Nonuniform polar grid algorithm for fast field evaluation," *IEEE Antennas Wireless Propag. Lett.,* vol. 1, no. 1, pp. 142–145, 2002.
[37] MATLAB R2016a, The MathWorks, Natick, 2016.
[38] Timothy A. Davis, "Direct Methods for Sparse Linear Systems," *SIAM,* Philadelphia, Sept. 2006. DOI: http://dx.doi.org/10.1137/1.9780898718881.
[39] C. Balanis, "Advanced Engineering Electromagnetics," *Wiley*, 1989.
[40] C. Craeye, B. Parvais and X. Dardenne, "MoM simulation of signal-to-noise patterns in infinite and finite receiving antenna arrays," *IEEE Trans. Antennas Propag.,* vol. 52, no. 12, pp. 3245–3256, Dec. 2004.
[41] K. F. Warnick, M. V. Ivashina, R. Maaskant and B. Woestenburg, "Unified Definitions of Efficiencies and System Noise Temperature for Receiving Antenna Arrays," *IEEE Trans. Antennas Propag.,* vol. 58, no. 6, pp. 2121–2125, June 2010.
[42] T. Clavier et al., "A Global-Local Synthesis Approach for Large Non-Regular Arrays," *IEEE Trans. Antennas Propag.,* vol. 62, no. 4, pp. 1596-1606, April 2014.
[43] A. J. Poggio, E. K. Miller, R. Mittra, "Integral equation solutions of three-dimensional scattering problems," Computer Techniques for Electromagnetics, Oxford, UK:Pergamon Press, 1973.
[44] C. Craeye, T. Gilles and X. Dardenne, "Efficient full-wave characterization of arrays of antennas embedded in finite dielectric volumes," *Radio Sci.,* vol. 44, no. 01, pp. 1–12, Feb. 2009.

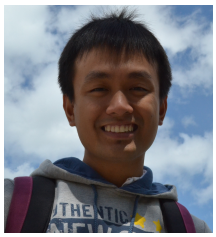

Ha Van Bui received the Engineering degree from Hanoi University of Technology, Vietnam in 2010 and the PhD in Electrical Engineering from Politecnico di Milano, Italy in 2014. From January to August 2014, he was a research assistant at Politecnico di Torino, Italy. Since September 2014, he has been with the antenna group, ICTEAM, Université catholique de Louvain (UCL) as a postdoctoral researcher. His research interests include the study of mutual coupling in antenna arrays, fast simulation techniques for large irregular arrays including the Square Kilometer Arrays (SKA-low and SKA-mid), and array optimizations.

Jens Abraham received the Dipl.Ing. degree in Electrical Engineering from TU Dresden, Dresden, Germany, in 2015. He was research assistant with the Astrophysics Group, Cavendish Laboratory, University of Cambridge, Cambridge, UK, from 2015 to 2017, and is PhD fellow with the Department of Electronics, Norwegian University of Science and Technology, Trondheim, Norway, since 2017. His current research interests include measurements and modeling of massive MIMO radio channels.

Michel Arts was born in Deurne, the Netherlands on February 21st 1968. In 1992 he received his M.Sc degree in electrical engineering from the Eindhoven University of Technology. From 1993 to 1995 he did a post-M.Sc program Information and communication technology at the Stan Ackermans Institute of the Eindhoven University of Technology. Since 1995 he works as an antenna design engineer at the Netherlands Institute for Radio Astronomy (ASTRON) in Dwingeloo, the Netherlands. There he worked on several projects like LOFAR (LOw Frequency ARray), the phased array demonstrators THEA (THousand Element Array) and EMBRACE (Electronic Multi-Beam Radio Astronomy ConcEpt) and the phased array feed for the Westerbork Synthesis Radio Telescope. His research interests include array modeling and phased array design for radio astronomy.

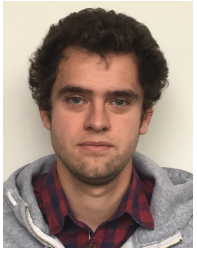

Quentin Gueuning received the B. Sc. and the M.Sc. degrees in Université catholique de Louvain (UCL), Louvain-La-Neuve, Belgium, in 2012 and 2014 respectively. Since 2014, he is working as a Research Assistant and pursuing a PhD Thesis in the Institute of Information and Communication Technologies, Electronics and Applied Mathematics (ICTEAM) in UCL. His main domains of interest include high-frequency and fast numerical methods for electromagnetic radiation.

Christopher Raucy obtained his degree in electromechanical engineering from Ecole Polytechnique de Louvain in 2011. Then, he worked at UCL for a year on the Square Kilometre Array (SKA) in collaboration with the University of Cambridge. In 2012 he started his PhD on the Myrrha RFQ simulation with the MoM for the next four years. In parallel with his PhD, he obtained a degree in Mathematics from Ecole Mathmatique de Louvain. He has also many interests in electronics and fundamental physics.

David González-Ovejero (S'01 – M'13 – SM'17) was born in Gandía, Spain, in 1982. He received the telecommunication engineering degree from the Universidad Politécnica de Valencia, Valencia, Spain, in 2005, and the Ph.D. degree in electrical engineering from the Université catholique de Louvain, Louvain-la-Neuve, Belgium, in 2012.

From 2006 to 2007, he was as a Research Assistant with the Universidad Politécnica de Valencia. In 2007, he joined the Université catholique de Louvain, where he was a Research Assistant until 2012. From 2012 to 2014, he worked as Research Associate at the University of Siena, Siena, Italy. In 2014, he joined the Jet Propulsion Laboratory, California Institute of Technology, Pasadena, CA, USA, where he was a Marie Curie Postdoctoral Fellow until 2016. Since then, he has been a Research Scientist with the French National Center for Scientific Research (CNRS), appointed at the Institut d'Electronique et de Télécommunications de Rennes, France.

Dr. González-Ovejero was a recipient of a Marie Curie International Outgoing Fellowship from the European Commission 2013, the Sergei A. Schelkunoff Transactions Prize Paper Award from the IEEE Antennas and Propagation Society in 2016, and the Best Paper Award in Antenna Design and Applications at the 11th European Conference on Antennas and Propagation in 2017.

Eloy de Lera Acedo (PhD'10) is a senior research fellow with the Cavendish Astrophysics group where he has developed his career on instrumentation for radio astrophysics. Eloy's research interest ranges from ultra wideband array and antenna design, electromagnetic modeling, telescope calibration, low noise systems to the broader science case of 21-cm cosmology experiments. Eloy leads the Novel Sensors research group at Cavendish Astrophysics and leads the Antenna and LNA Work package (AL WP) of the Aperture Array Design Consortium, which is developing the array stations for the SKA telescope. Within the AL WP Eloy has led the design and development of SKALA, the SKA Log periodic Antenna and its LNA. Eloy has also lead substantial pieces of work in other international projects such as the Hydrogen Epoch of Re-ionization Array (HERA) for which he has led the design of the wide band feed within the analogue team group.

Christophe Craeye (M'98 – SM'11) was born in Belgium in 1971. He received the Electrical Engineering and Bachelor in Philosophy degrees and the Ph.D. degree in applied sciences from the Université catholique de Louvain (UCL), Louvain-la-Neuve, Belgium, in 1994 and 1998, respectively. From 1994 to 1999, he was a Teaching Assistant with UCL and carried out research on the radar signature of the sea surface perturbed by rain, in collaboration with NASA and ESA. From 1999 to 2001, he was a Postdoctoral Researcher with the Eindhoven University of Technology, Eindhoven, The Netherlands. His research there was related to wideband phased arrays devoted to the square kilometer array radio telescope. In this framework, he was also with the University of Massachusetts, Amherst, MA, USA, in the Fall of 1999, and was with the Netherlands Institute for Research in Astronomy, Dwingeloo, The Netherlands, in 2001. In 2002, he started an antenna research activity at the Universite catholique de Louvain, where he is now a Professor. He was with the Astrophysics and Detectors Group, University of Cambridge, Cambridge, U.K., from January to August 2011. His research is funded by Région Wallonne, European Commission, ESA, FNRS, and UCL. His research interests include finite antenna arrays, wideband antennas, small antennas, metamaterials, and numerical methods for fields in periodic media, with applications to communication and sensing systems. Prof. Craeye was an Associate Editor of the *IEEE Transactions on Antennas and Propagation* from 2004 to 2010. He currently serves as an Associate Editor of the *IEEE Antennas and Wireless Propagation Letters*. In 2009, he was the recipient of the 2005-2008 Georges Vanderlinden Prize from the Belgian Royal Academy of Sciences.